# Structural Analyses of the JLab Hall D Replacement Solenoid

Craig E. Miller and Alexey Radovinsky

***Abstract*—The conceptual design of the replacement solenoid for the 12 GeV upgrade at Jefferson Lab is analyzed structurally. First, stress distributions within a detailed cross-section of the winding pack under Lorentz and thermal loads are discussed. These stress distributions are used to evaluate the integrity of the copper conductor and fiberglass insulation. Slip planes are included between the ground insulation of each coil and the mandrel. Second, the design of the support rods that carry the axial EM forces attracting the cold mass to the iron, carry the weight of the cold mass and provide lateral elastic stiffness offsetting attraction of the cold mass to the iron yoke in the event the cold mass is not concentric with the iron yoke is also presented. Third, the integrity of the cryostat is evaluated while bearing loads from the cold mass supports, the attraction of the cold mass to the iron yoke, atmospheric pressure, and the step-stops preventing cryostat axial displacements. Fourth, the stresses in the conductor during winding are evaluated.**

***Index Terms*—Cold mass support sizing, conductor winding tension, cryostat structural analysis, finite-element analysis, superconducting magnet.**

## I. Introduction

THE STRUCTURAL analysis of the conceptual design for a replacement solenoid for use in Hall D of the Laboratory at Thomas Jefferson National Accelerator Laboratory (JLAB) is presented for use in the 12 GeV program. The conceptual design has been outlined [1] to replace the existing magnet consisting of four separate toroidal coils and cryostats following the design goals in [2]. The intent is to integrate the existing iron yoke into a new magnet design that meets the field requirements and spatial constraints. The 1010 Steel yoke is a tube with 4.65 m length, 1.85 m inside diameter, and 3.76 m outside diameter is described in detail in [2].

## II. Cold Mass Analysis

### A. Geometry

The solenoid consists of three winding packs, each winding pack is wound on a separate mandrel and the three mandrels are connected using cylindrical spacers. The solenoid is shown in Fig. 1. The stress analysis on the cold mass couples Lorentz forces imported from an Electro-Magnetic (EM) analysis together with thermal loads. The axial symmetry of the solenoid is taken advantage of by reducing the Finite Element Model (FEM) to 2D. Fig. 2 shows the meshed conductor geometry. There are two main differences between Fig. 2 and the actual geometry: (1) is the smeared material representing the superconducting wires and solder and (2) is the sharp corners of the copper conductor used in the FEA. The latter of the two prevents increased mesh density for the model, but can lead to numerical problems where the orthogonal turn wrap orientations converge. The various materials used in the FEA are labeled in Fig. 2 and described in Table I.

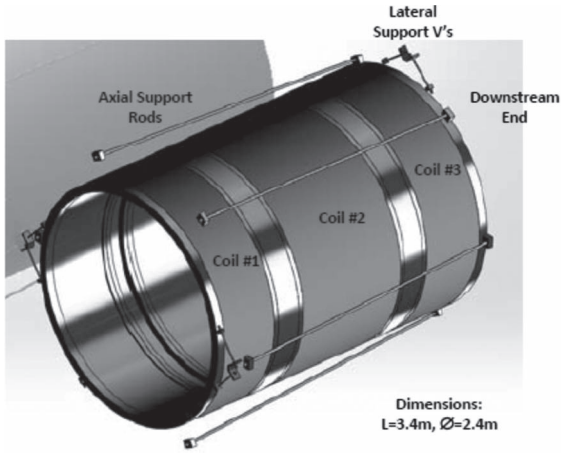


Fig. 1. 3-D model of three solenoids on mandrel showing axial and lateral cold mass support rods.

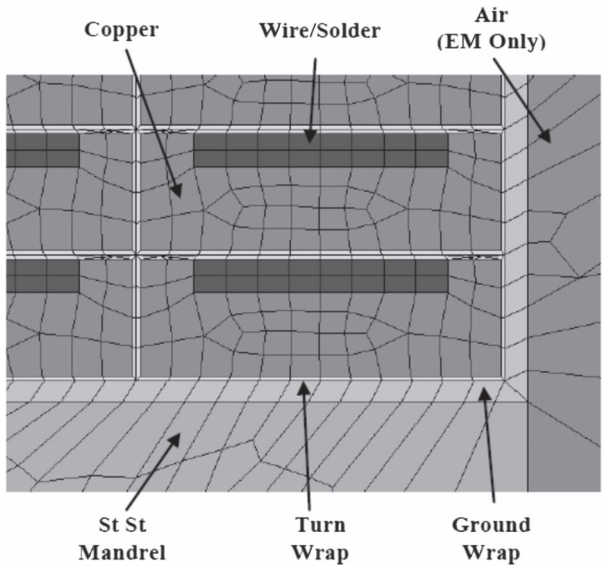


Fig. 2. Corner of meshed winding pack used for the 2D axi-symmetric FEM. Fig. zooms to Coil #3 at upstream end along outside diameter.

Manuscript received October 2, 2012; accepted November 21, 2012. Date of publication November 29, 2012; date of current version January 12, 2013. This work was supported in part by Jefferson Science Associates, LLC under U.S. DOE Contract DE-AC05-06OR23177.

The athors are with MIT-Plasma Science and Fusion Center, Cambridge, MA 02139 USA (e-mail: cemiller@psfc.mit.edu; radovinsky@psfc.mit.edu).

Digital Object Identifier 10.1109/TASC.2012.2230676

1051-8223/$31.00 © 2012 IEEE

TABLE I
TEMPERATURE DEPENDENT MATERIAL PROPERTIES USED IN FEA

| Material | Temperature (K) | Secant CTE ($10^{-6}$/K) | Elastic Modulus ($10^9$ Pa) | Poisson's Ratio |
|---|---|---|---|---|
| Copper | 295 | 11.4 [3] | 129 [4] | 0.31 [4] |
| | 4 | 0 | 138 [4] | |
| St. Steel 316LN | 295 | 10.3 [3] | 194 [3] | 0.25 [5] |
| | 4 | 0 | 205 [3] | |
| Smeared Solder/Wire | 295 | 11.3 [6] | 78.2 [7],[8] | 0.37 |
| | 4 | 0 | 97.2 [7],[8] | |
| G-10CR in-plane | 295 | 8.32 [3] | 22 [9],[10] | 0.25 [11] |
| | 4 | 0 | 27 [9],[10] | 0.36 [11] |
| G-10CR normal | 295 | 24.4 [3] | 14 [9],[10] | 0.15 [11] |
| | 4 | 0 | 22 [9],[10] | 0.25 [11] |

Slip planes between the ground wrap and the mandrel are included in the FEM using contact elements. Contact elements allow for compressive load transfer, $N$, shear load transfer up to $F_{MAX} = \mu N$, and separation if tensile loads are present, where $\mu$ is the friction coefficient. Once the shear load, or frictional force, reaches $F_{MAX}$, it cannot increase any further and the coil will slip against the mandrel.

### B. Material Properties

All materials in the FEM are isotropic, except the fiberglass which is transversely isotropic. The cable in copper channel conductor is modeled with 20% cold worked Oxygen-Free High thermal Conductivity (OFHC) copper for the channel and smearing isotropic superconducting strands and solder properties for the SSC outer cable. The averaging of the wire/solder material properties is weighted to the percentage of the cross sectional area that each material takes, using the standard rule-of-mixtures formula. It is assumed that eutectic Sn-Pb solder is used to attach 36 strands of Nb-Ti/Cu superconducting composite wire into the copper channel.

Both the ground wrap and turn wrap insulation use G10CR material properties. There is much confusion in the literature regarding proper laminate property orientation. Here it is assumed that the fiberglass is a transversely isotropic plate, where the normal direction is orientated through the thickness of the plate. The transverse wrap and fill directions are smeared for the in-plane material properties.

The mandrel is 316 stainless steel and the iron yoke is 1010 steel, with a 64 point BH curve used in the EM analysis.

### C. Loads and Boundary Conditions

Thermal loads are coupled with EM loads to generate the stress distributions in the solenoid. The EM loads are created by applying a $302 \times 10^6$ A/m$^2$ current density normal to each smeared area in the solenoid. The thermal loads are evaluated using a uniform temperature of 4 K. The process step of curing the epoxy around the wrapped coils is not included here. In order to use the epoxy cure temperature of 150 C as the structure's zero-stress temperature, the geometry at 150 C would need to be input as well as the mechanical response of the materials up to 150 C. The epoxy will most likely have a large plastic component to its behavior at these higher temperatures. Therefore, all data presented in the subsequent discussion implements a uniform zero-stress temperature of 295 K.

### D. Structural Results

It was found that for $\mu < 0.5$, one end and the inner diameter of each coil will separate from the mandrel and the opposite end of each coil will slip on the mandrel. Therefore, the critical stresses to be evaluated are: (1) the stress intensity, $S_{int}$, of the conductor to ensure it will be self-supporting, and (2) the integrity of the turn and ground insulation. The former is used here because pressure vessel design criteria are commonly compared to $S_{int} = \text{MAX}[|S_1 - S_2|, |S_2 - S_3|, |S_1 - S_3|]$, where $S_{1,2,3}$ are the principal stresses [12]. The latter includes quantifying the amount of tension normal to the fiberglass surface and formulating an allowable shear stress on the fiberglass surface. It is critical to minimize tension and shear stresses in the winding pack that cause delamination leading to possible coil quench conditions.

Fig. 3 captures the peak stress level in the copper channel as 131 MPa, which is less than the maximum allowable stress for copper of 150 MPa. Further investigation of Fig. 3 indicates the source of the high stresses in the conductor is the hoop stress. This hoop stress is due to the conductor supporting the Lorentz forces. The second source of these stresses is the axial stress due to the bending of the coils. This bending is due to the frictional force between each coil and the mandrel.

Slippage between the winding packs and the mandrel draw concern due to the shear stress acting on the fiberglass ground wrap. Coil #3 bears the largest axial force, so it also has the largest frictional force, hence shear stress. The shear stress on the interface is less than 5 MPa, which is not a concerning stress level.

The turn and ground insulation is evaluated using a combination of the normal and shear stresses. It is assumed that any tensile normal load will lead to cracks and/or delamination of the fiberglass material. Also, the lap shear strength is compared to a combination of the shear and normal stresses. For example, a high compressive stress in the presence of a high shear can act to prevent shear failure. Greater than 97% of the ground and turn insulation pass both the normal and shear failure criteria, which, from our experience of designing and fabricating similar systems, is deemed to be acceptable.

### E. Thermal Results

As previously discussed, each of the three coils will slip continuously during charging of the coils. The nonlinearities of the forces prior to saturation of the iron are neglected here. Also, it is important to note that there may be some slip-stick events between the coils and mandrel during initial training of the system. Once the coils have worked against the mandrel, it is assumed that the slip will occur continuously while the coils are being charged for one hour.

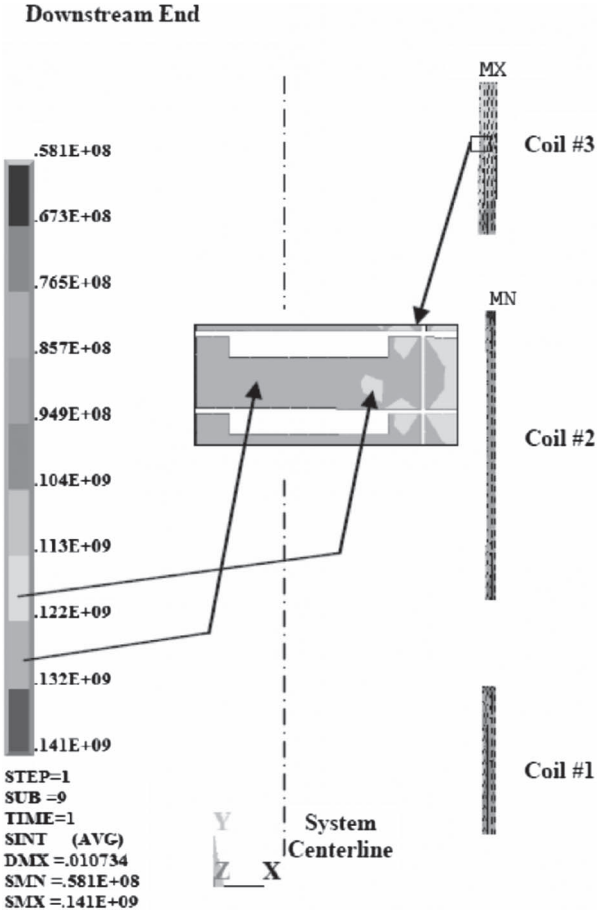


Fig. 3. Stress intensity of copper channel in winding pack. Inset zooms to location of highest stress intensity—along the ID of Coil #3.

The energy (power) each coil will dissipate over this one hour charge is:

- Coil $1 = 159$ Joules (0.0442 Watts),
- Coil $2 = 40.4$ Joules (0.012 Watts),
- Coil $3 = 39.6$ Joules (0.011 Watts).

These data points are used as power input to a steady-state thermal FEM with the same mesh as previously discussed. It is assumed that this power is input continuously using $F_{MAX}$ when the coils are fully charged. Therefore, these are conservative results because most slippage occurs before the coil is fully charged when the forces are lower.

The resulting temperature distributions indicate $< 0.1$ K temperature increase in the winding due to the slipping of the coils occurring during the one hour charge time. This is comfortably below the 1.5 K temperature rise that would place the conductor at the current sharing temperature at the maximum field location in the winding.

## III. Cold Mass Support Rods

Fig. 1 includes the warm-to-cold rods supporting the cold mass from the room temperature cryostat. The scheme consists of : (1) axial support rods carry EM forces attracting the cold mass to the downstream end of the iron yoke in the axial direction, and (2) lateral support rods installed in four V-shaped arrangements at the ends of the cold mass that serve two purposes. First, they carry the weight of the cold mass. Second, when the axes of the cold mass and the iron are misaligned, they provide elastic stiffness in the lateral direction to offset the positive magnetic stiffness caused by the EM attraction between the iron yoke and the energized coil.

### A. Axial Supports

The axial force of attraction of the cold mass to the downstream, high field end of the iron yoke is 1.24 MN. Using a safety factor of 3, and assuming the rods are made of Nitronic 50 stainless steel, either six 2.54 cm diameter rods, or eight 2.22 cm diameter rods can be safely used to bear the axial force. The six rod choice is given preference due to its relative simplicity to implement.

### B. Lateral Supports

The lateral cold mass support is provided by eight rods, grouped in four V-shaped arrangements as shown in Fig. 1. The lateral supports are sized by strength and stiffness and the design uses the worst case of the two approaches. In order to provide uniform elastic stiffness in all lateral directions all support rods must be preloaded in tension. Therefore, the rods will be in tension under any load conditions.

To guarantee that the rods always stay in tension it is assumed that the tensile preload shall be at least 1.5 times the portion of the weight each bears. In the analyses it is assumed that the weight of the cold mass is uniformly distributed among all four V's. Using a safety factor of 3, the lateral support rods should have a 12.7 mm diameter when being sized by strength.

Positive magnet stiffness in the lateral direction was calculated using the forces on the cold mass resulting from being shifted in the lateral direction within the iron yoke. These forces are applied to the lateral V-supports as a function of the lateral displacement of the cold mass. Using a safety factor of 3, it is found that the 12.7 mm diameter rods will satisfy both the mechanical strength and magnetic stiffness considerations.

## IV. Cryostat

The cryostat encases the vacuum surrounding the cold mass and it bears loads from: (1) tension in cold mass support V's, (2) axial loads from the attraction of the cold mass to the downstream end of the iron, (3) atmospheric pressure on the outside and vacuum on its inside, and (4) the step-stops preventing cryostat axial displacements. The step-stops are tabs attached to the cryostat shell and engage the iron yoke—without them the loads from the six axial support rods would buckle the cryostat shell.

The cryostat FEA implements shell elements of 304 stainless steel that are 15 mm thick for the full 3D geometry. The step-stops and chimney (used to route current leads and cooling lines) are modeled using 3D brick elements. Forces are applied on the four step-stops that are equal and opposite to the forces in the six axial support rods. Contact between the iron yoke and the cryostat is simulated using elastic foundation.

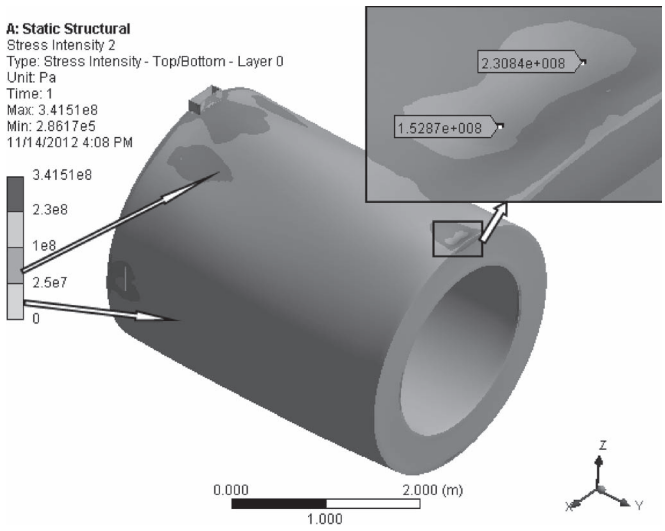


Fig. 4. Stress intensity of the cryostat. Inset shows peak stresses where lateral support V's converge with contact to cryostat at downstream end.

The stress intensity is used to evaluate the integrity of the cryostat under these loads to ensure it does not rupture and to ensure the step-stops do not break away. The map of the Cryostat stress intensity is shown in Fig. 4. The stress intensity scale is set so that any stresses higher than the allowable stress of 230 MPa are black. The step-stops on the sides of the cryostat have highest stresses because they coincide with locations of the lateral support V's. The peak stress of 231 MPa is marked in the top right inset of Fig. 4 and these can be reduced in a detailed design by proper sizing of the brackets used to connect the support rods to the cryostat. Stresses in the remainder of the cryostat remain very low, less than 109 MPa.

## V. Tension in Conductor During Winding

The conductor will be loaded in tension during the winding process so that it will conform to the inner radius of the mandrel. The magnitude of the tension is important to ensure it is not large enough to damage the conductor during the winding process. An analytical approach is used to determine the tension and this value is used in a FEM to predict the conductor stress. The analytical approach assumes a length of the conductor bends to conform to 1/4 of the mandrel circumference behaves similar to a beam. The equation for a fixed-fixed beam bearing a distributed load is implemented: $\delta_{max} = (w_o.L^4)/(384 \cdot EI)$, where $w_o$ is the contact force from the mandrel and $E, L, I$ are the stiffness, length and moment of inertia of the conductor [13]. Assuming the conductor is solid copper, the winding tension, $T$, is: $T = 820$ N $= 184$ lb.

A bilinear elastic-plastic FEA is used to observe how well the conductor conforms to the mandrel with the 820 N winding tension. The FEM consists of 1/4 of the mandrel having equal thickness to a single turn of the conductor and a conductor of solid copper. The mandrel is rigid, one end of the conductor is fixed to the mandrel and the winding tension is applied to the other end. Frictionless contact is applied between the conductor and mandrel.

The results indicate that after the 1/4 turn, 85% of the conductor is in contact with the 2.2 m diameter mandrel and the peak separation is only 0.025 m. It is important to note that very large winding tensions ($T = 1500$ N) only reduced the maximum separation to 15 mm. It is also important to note that there is significant spring-back of the conductor after the tension is released, so that clamps must be properly designed to prevent this spring back during the winding operation.

The winding tension creates various stress fields as the conductor is wound. First, the longitudinal stress of 10.7 MPa is very low compared to the 275 MPa yield stress and of little concern, even with deviations in winding tension. The stress intensity at the perimeter of the conductor is 280 MPa. This is greater than the yield strength (necessary to conform the conductor to the mandrel), but less than the tensile strength of 290 MPa.

## VI. Conclusion

The conceptual design of the replacement solenoid in Hall D of JLAB is analyzed structurally. Data from the analyses indicate the design is safely below the failure criteria for the cold mass, warm-to-cold support rods and cryostat. The data also indicate the winding tension is sufficient to keep conductor in contact with mandrel, but will not break the conductor during manufacturing. With this level of confidence, the conceptual design moves to the detailed design stage of the overall project.

## References

[1] B. Smith *et al.*, "Conceptual design of the JLab Hall D replacement solenoid," presented at the Appl. Supercond. Conf., 2012, Paper no. 2JPA-11.
[2] G. Biallas *et al.*, "Design goals for Hall D replacement solenoid," Nov. 4, 2010, GlueX-doc-1634.
[3] [Online]. Available: http://cryogenics.nist.gov/MPropsMAY/material%20properties.htm
[4] N. J. Simon, E. Drexler, and R. Reed, "Properties of copper and copper alloys at cryogenic temperatures," *NIST Monograph 177*, Feb. 1992.
[5] [Online]. Available: www.matweb.com
[6] Y. Iwasa, *Case Studies in Superconducting Magnets*. New York: Springer, 2009, p. 638.
[7] M. Fink *et al.*, "Measurement of mechanical properties of electronic materials at temperatures down to 4.2 K," *Cryogenics*, vol. 48, pp. 497–510, 2008.
[8] D. T. Read and H. M. Ledbetter, "Temperature dependence of the elastic constants of an NbTi/Cu superconducting composite," *Composites*, Apr. 1978.
[9] R. P. Reed and A. F. Cark, "Material at low temperatures," *ASM*, 1983.
[10] Y. Shindo *et al.*, "Cryomechanics and short-beam interlaminar shear strength of G-10CR glass-cloth/epoxy laminates," *Adv. Cryogen. Eng.*, vol. 46A, p. 167, 1999.
[11] M. B. Kasen *et al.*, "Mechanical, electrical and thermal characterization of G-10CR and G-11CR glass-cloth/epoxy laminates between room temperature and 4 K," *Adv. Cryogen. Eng.*, vol. 26, p. 235, 1979.
[12] S. Chattopadhyay, *Pressure Vessels: Design and Practice*. Boca Raton, FL: CRC Press, 2005.
[13] R. D. Cook and W. C. Young, *Advanced Mechanics of Materials*. New York: MacMillan, 1985.